Approach for Targeting Landers and Penetrators Using Orbital Optical Navigation

Tseng-Chan Wang,* Thomas C. Duxbury,† and Stephen P. Synnott‡
Jet Propulsion Laboratory, California Institute of Technology, Pasadena, California 91109
and
Kathleen Edwards§
U.S. Geological Survey, Flagstaff, Arizona 86001

A new approach for targeting landers, rovers, and penetrators to specific points on the surfaces of planetary bodies using onboard, orbital optical navigation data is presented. Earth-based radiometric tracking of the orbiting spacecraft provides a very precise determination of the spacecraft orbit about the primary planetary body. Onboard optical navigation images are then used to relate the spacecraft orbit to the surface of the target body. This paper concentrates on the problem associated with using the onboard optical navigation data, which will have to estimate, in a near-real time orbit determination process, a large set of parameters including the spacecraft orbit and primary body gravity field, the rotational properties of the planetary body, the coordinates of surface features, and the camera pointing and orientation of each picture. A batch-sequential formulation of the standard least squares problem is used with the addition of backward smoothing. A square-root information filter is also used for numerical precision and stability and to minimize computer memory. To illustrate this approach, over 100 images of Phobos were processed to estimate about 2000 parameters including the camera pointing angles, the rotational properties of Phobos, and the locations of surface features.

Nomenclature

$\bar{a}$	= surface feature position vector with respect to spacecraft in B1950
$\bar{b}$	= surface feature position vector with respect to Phobos center in B1950
b_X, b_Y, b_Z	= components of $\bar{b}$ along the axes of the B1950 system
C	= camera pointing parameters
d	= surface feature position vector in camera-fixed coordinate system
d_x, d_y, d_z	= components of d along the axes of camera-fixed coordinates
f	= camera focal length
I_X, I_Y	= identity matrices corresponding to sizes of X and Y, respectively
j	= batch number
$(\ )_j$	= given quantity is associated with batch j
K	= transformation matrix from vidicon coordinates to sample and line coordinates
M	= diagonal transition matrix
N	= total number of batches
nc	= number of control points processed
ng	= number of grid points used for generating a contour map
np	= number of stochastic parameters
P	= stochastic parameters
$\tilde{P}$	= smoothed stochastic parameters
p	= given stochastic parameter in P
$\tilde{p}$	= given smoothed stochastic parameter in $\tilde{P}$
$R_C, R_{\hat{X}}, R_Y$	= elements of the upper triangular square-root information matrix corresponding to C, $\hat{X}$, and Y, respectively
$R_{C\hat{X}}, R_{CY}, R_{\hat{X}Y}$	= cross elements of the upper triangular square-root information matrix associated with C, $\hat{X}$, and Y, respectively
R_{C0}	= a priori information matrix for camera pointing parameters
R_X, R_P, R_Y	= elements of the upper triangular square-root information matrix corresponding to X, P, and Y, respectively
R_{XP}, R_{XY}, R_{PY}	= cross elements of the upper triangular square-root information matrix associated with X, P, and Y
$R_{\hat{X}0}$	= a priori information matrix for spacecraft state parameters
$(R^*_{pX}\, r^*_{pp}\, R^*_{pY})_j$	= smoothing coefficients for $\tilde{p}$ in batch j associated with $(\hat{X}\ \tilde{p}\ Y)^T$ in batch $(j+1)$
$\bar{s}$	= Phobos position vector with respect to Mars in B1950
s, l	= sample and line (image) coordinates
s_0, l_0	= image coordinates of the central reseau
T^I_{BF}	= transformation matrix from B1950 to body-fixed coordinates
T^{BF}_I	= transformation matrix from body-fixed coordinates to B1950
T^I_{TV}	= transformation matrix from B1950 to camera-fixed coordinates
$(\ )^T$	= transpose of a matrix
$\bar{t}$	= Phobos position vector with respect to spacecraft in B1950
t_N	= final time
t_0	= epoch time
$\bar{u}$	= Phobos center position vector to the surface of a control point in body-fixed $\bar{x}\bar{y}\bar{z}$ coordinate system
$\hat{u}$	= unit vector of $\bar{u}$

Presented as Paper AAS 89-404 at the AAS/AIAA Astrodynamics Specialist Conference, Stowe, VT, Aug. 7-10, 1989; received Dec. 28, 1989; revision received June 19, 1990; accepted for publication Sept. 12, 1990.

*Member of Technical Staff, Mail Stop 301-220G, Navigation Systems Section, 4800 Oak Grove Drive.
†Senior Scientist, Mail Stop 183-501, Earth and Space Sciences Division, 4800 Oak Grove Drive.
‡Optical Systems Analysis Group Supervisor, Mail Stop 301-125L, Navigation Systems Section, 4800 Oak Grove Drive.
§Cartographer, Branch of Astrogeology, 2255 N. Gemini Drive.

u = radius to the control point on the surface
$u_{\bar{x}}, u_{\bar{y}}, u_{\bar{z}}$ = components of $\bar{u}$ along the axes of body-fixed coordinates
$V_P(j)$ = matrix of partials of the spacecraft state with respect to parameters P from batch j to batch $(j+1)$
w = filter process noise that derives the colored noise
X = spacecraft pseudoepoch state corrections
$\tilde{X}$ = smoothed spacecraft pseudoepoch state corrections
$\hat{X}$ = spacecraft current epoch state corrections
$\bar{X}\bar{Y}\bar{Z}$ = IAU standard Earth Mean Equator and Equinox of Besselian 1950.0 inertial reference system (referred to as B1950)
$\bar{x}$ = spacecraft position vector with respect to Mars in B1950
xyz = camera-fixed coordinate system
$\bar{x}\bar{y}\bar{z}$ = body-fixed coordinate system
x, y = vidicon coordinates in mm space
Y = bias parameters
$z_C, z_{\hat{X}}, z_Y$ = adjusted residual vectors corresponding to C, $\hat{X}$, and Y, respectively
z_X, z_P, z_Y = adjusted residual vectors corresponding to X, P, and Y, respectively
z_w^* = smoothing coefficient for $\tilde{p}$ associated with the normalized process noise estimate
α, δ, W = pole and prime meridian parameters
$\alpha_c, \delta_c, \kappa$ = camera pointing and orientation angles
Γ = error covariance of the estimated bias parameters
Δt_j = delta time from t_j to t_{j+1}
Λ_i = error covariance derived from Γ for the ith control point
σ_i = uncertainty of the ith control point
σ_k = uncertainty computed for the kth grid point
σ_p^* = smoothing coefficient for $\tilde{p}$
τ_k = correlation time for the kth stochastic parameter
ϑ_{ik} = angle between the ith control point unit position vector and the kth grid point unit position vector
ϕ, λ = cartographic latitude and longitude of a control point
Ψ_i = mapped error covariance for the ith control point

Introduction

CURRENT and future planetary missions will involve the delivery of landers, rovers, and penetrators to specific points on the surfaces of planetary bodies. These missions include the Soviet Phobos 88 mission, which was planned to place a short-term hopper and a long-term lander on Phobos, the Comet Rendezvous and Asteroid Flyby[1] (CRAF) mission, which will place penetrators into the surface of a comet, and the Soviet Mars 94 and U.S. Mars Rover Sample Return[2] (MRSR) missions, which will place landers and rovers on Mars.

The safety and survivability of these probes to the surface will depend on first selecting safe landing sites and then precisely targeting the probes to specific points on the surface and performing terminal guidance to land at these points.[1,3] Both CRAF and MRSR have topographic accuracy requirements at the meter level[1,4] in their penetrator and rover landing sites. This level of accuracy can be used to register high resolution and remote observations of the landing sites, select safe landing sites, control the descent, and select rover traverse paths.

Earth-based radiometric tracking [e.g., two- and three-way Doppler, ranging, very long baseline interferometry (VLBI)] of the orbiting spacecraft carrying the landers/rovers/penetrators provides a very precise determination of the spacecraft orbit about the primary planetary body (e.g., Mars, a comet). Onboard optical navigation images are then used to relate the spacecraft orbit to the surface of the target body. Also, in the case of Phobos 88, it was planned to use the optical data to tie the orbit of the spacecraft about Mars to both the orbit of Phobos and the surface of Phobos.

This paper concentrates on the problem associated with using the onboard optical navigation data. The optical data will be used to produce cartographic map products, which include topography, boulder sizes, and the distribution and the location of other hazards to assess the relative safety and traversability of various landing sites. Relative topographic information is more important than absolute information in this application. Once a landing site is selected, the absolute, inertial coordinates of the spacecraft orbit and desired landing point are used to target the probes to the surface. Once deployed, MRSR may use a terminal guidance scheme that uses a precomputed map of the desired landing site to control the landing to a safe site by missing known boulders, crevasses, and areas having high slopes. Meter level topographic accuracies would be needed.

Problem Statement

The onboard orbital optical navigation data will have to estimate the following parameters in a near-real time orbit determination process.

1) The spacecraft orbit and primary body gravity field. The Earth-based radiometric tracking will be the primary data source for determining these parameters with the optical data providing additional refinement.

2) The orbit of a secondary body such as Phobos if the landing is to be on that body rather than the primary body.

3) The rotational properties of the planetary body including spin axis direction, rotation rate, precession, nutation, libration, pole wondering, wobble, etc., to relate the position and orientation of the surface to inertial space over time.

4) The body-fixed coordinates (e.g., latitude, longitude, radius) of surface control points (e.g., craters, boulders, albedo marks) used to produce maps of the landing sites.

5) The camera pointing and orientation of each picture.

The widely varying stochastic nature of these parameters and the total number of parameters to be estimated restrict the application of current techniques to this problem. A new approach is presented that takes advantage of the known stochastic characteristics of the problem to obtain a feasible solution; however, this solution will require a computer with the capability of today's supercomputer class to produce solutions within the near-real time mission operational time constraints.

Proposed Solution

The spacecraft orbit and primary body gravity field coefficients represent tens of parameters to be estimated. The gravity field coefficients are constant for all time and have no stochastic variation unless subsets of the total gravity field model are used. The spacecraft orbital parameters can be grouped in batches separated by orbit trim maneuvers causing orbit discontinuities or shorter arcs if a reduced gravity field model is used. Nongravitational forces acting on the spacecraft due to solar pressure or gas leaks have varying stochastic behaviors and may also place limits on batch sizes.

The rotational properties of planetary bodies have been modeled with constant parameters for past missions. However, when dealing with submeter observational accuracies of any planetary body or comet having a chaotic rotation,[5] rotational parameters (5–10 variables) may also have to be treated as stochastic processes.

The largest set of parameters to be estimated in the orbit determination process is the set of coordinates of surface fea-

tures. Three positional coordinates for each feature are needed, and with thousands to hundreds of thousands of features in the control network, one can easily fill the memory (nonvirtual) of any contemporary computer when attempting to manipulate the covariance associated with this problem. Therefore, a much smaller subset of features will be used to establish a global control network of the body and determine the rotational properties. Additional smaller, local control networks will be established at each potential landing site and processed separately, after the orbits and rotational parameters have been determined from the global control network.

Finally, three camera pointing angles are estimated for each picture. Using thousands of pictures for navigation makes this a large set of parameters to be estimated also. However, the pointing errors are completely random from picture to picture allowing a backward smoothed solution for these parameters to be produced after the main orbit determination process has been completed. This method provides a fully optimal solution of the camera pointing angles while not requiring these parameters to be in computer memory with the orbit determination process.

A batch-sequential formulation of the standard least squares problem will be used with the addition of backward smoothing.[6] A square-root information filter,[7] using Bierman's Estimation Subroutine Library,[8] will be used for numerical precision and stability and to minimize computer memory.

The time span for filter estimation is selected from t_0 to t_N, where t_0 is the epoch time and t_N the final time. This interval is subdivided into batches of varying time increments depending on the known stochastic characteristics of the problem and can be specified by the user. In the measurement updates, the a priori information about the uncertainties in the parameters being estimated is included as additional data to the information accumulation process. The Householder orthogonal transformations are applied to obtain an upper triangular square-root information matrix.[6,7]

The data equation for batch j in $t_{j-1} \le t < t_j$, where $0 < j \le N$, is given by

$$\begin{pmatrix} \boldsymbol{R}_X & \boldsymbol{R}_{XP} & \boldsymbol{R}_{XY} \\ 0 & \boldsymbol{R}_P & \boldsymbol{R}_{PY} \\ 0 & 0 & \boldsymbol{R}_Y \end{pmatrix}_j \begin{pmatrix} \boldsymbol{X}_j \\ \boldsymbol{P}_j \\ \boldsymbol{Y} \end{pmatrix} = \begin{pmatrix} z_X \\ z_P \\ z_Y \end{pmatrix}_j \tag{1}$$

where $\boldsymbol{R}$ are the associated elements of the upper triangular square-root information matrix with respect to parameters $\boldsymbol{X}$, $\boldsymbol{P}$, and $\boldsymbol{Y}$; $\boldsymbol{X}_j$ the spacecraft pseudoepoch state corrections for batch j; $\boldsymbol{P}_j$ the stochastic parameters that are piecewise constant having discontinuity at t_j; $\boldsymbol{Y}$ the bias parameters that have constant value over the entire time span; and z the adjusted residual vectors.

The system dynamics in terms of the pseudoepoch state formulation from batch j to batch $(j+1)$ are given as follows[6]:

$$\begin{pmatrix} \boldsymbol{X}_{j+1} \\ \boldsymbol{P}_{j+1} \\ \boldsymbol{Y} \end{pmatrix} = \begin{pmatrix} \boldsymbol{I}_X & \boldsymbol{V}_P(j) & 0 \\ 0 & \boldsymbol{M}_j & 0 \\ 0 & 0 & \boldsymbol{I}_Y \end{pmatrix} \begin{pmatrix} \boldsymbol{X}_j \\ \boldsymbol{P}_j \\ \boldsymbol{Y} \end{pmatrix} + \begin{pmatrix} 0 \\ \boldsymbol{w}_j \\ 0 \end{pmatrix} \tag{2}$$

where $\boldsymbol{w}_j$ is the filter process noise that derives the colored noise, and $\boldsymbol{M}_j$ is a diagonal transition matrix computed for each batch as follows:

$$\boldsymbol{M}_j = \operatorname{diag}\left[\exp(-\Delta t_j/\tau_1), \ldots, \exp(-\Delta t_j/\tau_{np})\right]$$

$\Delta t_j = t_{j+1} - t_j$, τ_k is the user input correlation time for the kth stochastic parameter, and np is the number of stochastic parameters. The matrix $\boldsymbol{V}_P(j)$ [i.e., $(\partial \boldsymbol{X}_{j+1}/\partial \boldsymbol{P}_j)_{P_j=0}$)] is the partials of the spacecraft state with respect to the parameters $\boldsymbol{P}$ from batch j to batch $(j+1)$. Equation (2) is used in the following two filter time updating processes in the order of deterministic update and then colored noise update.

Deterministic update:

$$\boldsymbol{X}_{j+1} = \boldsymbol{X}_j + \boldsymbol{V}_P(j)\boldsymbol{P}_j \tag{3}$$

Colored noise update:

$$\boldsymbol{P}_{j+1} = \boldsymbol{M}_j \boldsymbol{P}_j + \boldsymbol{w}_j \tag{4}$$

Let p_j be a stochastic parameter in $\boldsymbol{P}_j$. The results of the colored noise component update one at a time[7] for p_j are given as follows:

$$\sigma_p^* p_j + (R_{pX}^* r_{pp}^* R_{pY}^*) \begin{pmatrix} \boldsymbol{X}_{j+1} \\ p_{j+1} \\ \boldsymbol{Y} \end{pmatrix} = z_w^* \tag{5}$$

$$\begin{pmatrix} \boldsymbol{R}_X & \boldsymbol{R}_{Xp} & \boldsymbol{R}_{XY} \\ 0 & r_p & \boldsymbol{R}_{pY} \\ 0 & 0 & \boldsymbol{R}_Y \end{pmatrix}_{j+1} \begin{pmatrix} \boldsymbol{X}_{j+1} \\ p_{j+1} \\ \boldsymbol{Y} \end{pmatrix} = \begin{pmatrix} z_X \\ z_p \\ z_Y \end{pmatrix}_{j+1} \tag{6}$$

The coefficients with an * in Eq. (5) are saved for backward smoothing.

The algorithm for one colored noise component update at a time is applied to the succeeding stochastic parameters in $\boldsymbol{P}_j$ until the filter time updating process is completed. The measurement updates are then applied at the completion of the time updates for batch $(j+1)$. These two filtering procedures, measurement updates and time updates, are applied iteratively until the last requested batch N is processed.

Similar to the filter, the smoother operates in a backward recursive manner from the final batch N to the epoch of the first batch. The smoothed stochastic parameters $\tilde{\boldsymbol{P}}_j$ at batch j are determined by computing each smoothed stochastic parameter $\tilde{p}_j$ using the smoothing coefficients (with an *) saved in Eq. (5) and the smoothed estimate at batch $(j+1)$ as follows[6]:

$$\tilde{p}_j = \left(\frac{z_w^*}{\sigma_p^*}\right)_j - \frac{1}{(\sigma_p^*)_j} (R_{pX}^* r_{pp}^* R_{pY}^*)_j \begin{pmatrix} \tilde{\boldsymbol{X}}_{j+1} \\ \tilde{p}_{j+1} \\ \boldsymbol{Y} \end{pmatrix} \tag{7}$$

The resulting smoothed stochastic parameters $\tilde{\boldsymbol{P}}_j$ and the smoothed spacecraft state $\tilde{\boldsymbol{X}}_{j+1}$ at batch $(j+1)$ are used to compute the smoothed state at batch j by reversing the deterministic update from Eq. (3) as follows:

$$\tilde{\boldsymbol{X}}_j = \tilde{\boldsymbol{X}}_{j+1} - \boldsymbol{V}_P(j)\tilde{\boldsymbol{P}}_j \tag{8}$$

This completes the smoothed estimate step for batch j. Note that the bias parameters in $\boldsymbol{Y}$ are not changed in the smoothing process. The detailed recursion for the smoothed covariance reversing colored noise update and then deterministic update is given in Ref. 6.

The solution to the system of equations represented by Eqs. (1) and (2) will require the use of advanced radiometric tracking of the spacecraft from Earth (Doppler, ranging, VLBI, differential one-way range, etc.) as well as onboard optical, synthetic aperture radar, and possibly altimetry data. The onboard optical data used in this process would include limb/terminator observations to infer the target body center location and possibly a select few surface landmarks whose positions are well known.[9]

This paper pursues a method of taking the results of this process as a priori to processing hundreds to thousands of control points to produce high precision maps of potential landing sites that are accurately tied to inertial space and to the spacecraft trajectory. The separation of these two processes is proposed to keep the orbit determination task manageable and numerically stable. The processing of the control points separately represents a suboptimal approach, but it is felt that little accuracy is lost while substantial gains are made in numerical stability and ease of filter implementation for a problem involving thousands to tens of thousands of estimated parameters.

By separating the two processes, the second process can only concern itself with estimating small corrections to the spacecraft trajectory produced by the first process and does not include the difficult dynamic stochastic parameters (e.g., nongravitational forces) that were handled by the first process. Therefore, the second process, which is described in this paper, only estimates parameters that have constant values (the state transition matrix is an identity matrix) over the entire data set. Parameters like corrections to the spacecraft trajectory and camera pointing have fixed batch sizes and are handled as backward smoothed parameters to minimize the number of parameters being carried in the filter equations.

To effectively perform the second process, the data equation for the onboard optical observables is formulated as follows:

$$\begin{pmatrix} R_C & R_{C\hat{X}} & R_{CY} \\ 0 & R_{\hat{X}} & R_{\hat{X}Y} \\ 0 & 0 & R_Y \end{pmatrix} \begin{pmatrix} C \\ \hat{X} \\ Y \end{pmatrix} = \begin{pmatrix} z_C \\ z_{\hat{X}} \\ z_Y \end{pmatrix} \tag{9}$$

where R are associated elements of the upper triangular square-root information matrix with respect to parameters C, $\hat{X}$, and Y; C the corrections to the camera pointing angles; $\hat{X}$ the corrections to the current spacecraft state; Y the bias parameters that have constant values over the entire data set, such as pole and prime meridian parameters and coordinates of surface features; and z the adjusted residual vectors.

It is assumed that the corrections to camera pointing angles are independent from picture to picture. Therefore, the information related to camera pointing angles in Eq. (9) is saved at the end of processing each picture as follows:

$$(R_C \; R_{C\hat{X}} \; R_{CY}) \begin{pmatrix} C \\ \hat{X} \\ Y \end{pmatrix} = z_C \tag{10}$$

Equation (10) will be used in the backward smoothing process to obtain the camera pointing corrections for the corresponding pictures. After saving the information array in Eq. (10), the camera pointing information in Eq. (9) is reinitialized to continue data processing for the next picture as follows:

$$\begin{pmatrix} R_{C0} & 0 & 0 \\ 0 & R_{\hat{X}} & R_{\hat{X}Y} \\ 0 & 0 & R_Y \end{pmatrix} \begin{pmatrix} C \\ \hat{X} \\ Y \end{pmatrix} = \begin{pmatrix} 0 \\ z_{\hat{X}} \\ z_Y \end{pmatrix} \tag{11}$$

It is also assumed that the corrections to the current spacecraft state are independent from orbit to orbit. Therefore, the information related to spacecraft state in Eq. (9) is saved at the end of processing each spacecraft orbit as follows:

$$(R_{\hat{X}} \; R_{\hat{X}Y}) \begin{pmatrix} \hat{X} \\ Y \end{pmatrix} = z_{\hat{X}} \tag{12}$$

Equation (12) will be used in the backward smoothing process to obtain the corrections to the spacecraft state for the corresponding orbits. After saving the information array in Eq. (12), the information related to spacecraft state in Eq. (9) is reinitialized to continue data processing for the next orbit as follows:

$$\begin{pmatrix} R_{C0} & 0 & 0 \\ 0 & R_{\hat{X}0} & 0 \\ 0 & 0 & R_Y \end{pmatrix} \begin{pmatrix} C \\ \hat{X} \\ Y \end{pmatrix} = \begin{pmatrix} 0 \\ 0 \\ z_Y \end{pmatrix} \tag{13}$$

where $R_{\hat{X}0}$ is the a priori information matrix containing only diagonal elements for the spacecraft state. Note that Eq. (13) shows that the end of data processing for each spacecraft orbit coincides with the end of each picture processing.

After processing the entire data sets, the solutions for the estimated bias parameters Y are computed by

$$Y = R_Y^{-1} z_Y \tag{14}$$

and the covariance matrix Γ for Y is computed by

$$\Gamma = R_Y^{-1} R_Y^{-T} \tag{15}$$

By applying the backward smoothing process to the information saved in Eq. (12) and using the solution of Y in Eq. (14), the corrections to the spacecraft state for each orbit can be obtained as follows:

$$\hat{X} = R_{\hat{X}}^{-1}(z_{\hat{X}} - R_{\hat{X}Y} Y) \tag{16}$$

Similarly, applying the backward smoothing process to the information saved in Eq. (10) and using the solution of $\hat{X}$ (where the picture was taken) and Y in Eqs. (16) and (14), respectively, the camera pointing corrections for each picture can be obtained as follows:

$$C = R_C^{-1}(z_C - R_{C\hat{X}} \hat{X} - R_{CY} Y) \tag{17}$$

The technique of batching various parameters together and the use of the backward smoothing algorithm allow fully optimal solutions for most parameters while significantly reducing the amount of computer memory (virtual and nonvirtual). Future problems will need to solve for hundreds of thousands of parameters; however, only a few thousands of parameters will be resident in the computer's memory at a time.

Example

The following example was produced for Phobos, the inner moon of Mars, processing Viking Orbiter imaging data. Over 100 images of Phobos were processed to estimate about 2000 parameters including camera pointing, the rotational properties of Phobos, and the locations of surface features. These estimated results were used to generate cartographic map products useful for landing site selection.

Coordinate Systems

The following coordinate systems are established for processing surface feature images in the Phobos pictures taken by Viking Orbiter.

Body-Fixed Reference Coordinates

A body-fixed $\bar{x}\bar{y}\bar{z}$ coordinate system (Fig. 1), used to define the control points, is chosen to align with the three principal moments of inertia of Phobos.[10,11] In this system, $\bar{z}$ is along the spin axis, $\bar{x}$ is normal to $\bar{z}$ and in the direction of the longest axis and defines the prime meridian, and $\bar{y}$ completes the orthogonal, right-handed system.

Let $\bar{u}$ (in km) be a Phobos-centered position vector to the surface of a control point (e.g., crater, boulder, albedo mark) in $\bar{x}\bar{y}\bar{z}$ and it is expressed (see Fig. 1) in terms of cartographic

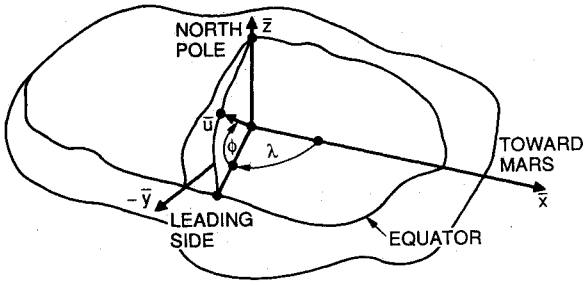

Fig. 1 Cartographic coordinates of a point on the surface of Phobos in body-fixed coordinate system.

latitude (ϕ, in deg) and longitude (λ, in deg) as follows:

$$\bar{u} = \begin{pmatrix} u_{\bar{x}} \\ u_{\bar{y}} \\ u_{\bar{z}} \end{pmatrix} = u \begin{pmatrix} \cos\phi \cos\lambda \\ -\cos\phi \sin\lambda \\ \sin\phi \end{pmatrix} = u\hat{u} \tag{18}$$

where $(u_{\bar{x}}\, u_{\bar{y}}\, u_{\bar{z}})^T$ are the components of $\bar{u}$ along the axes of $\bar{x}\bar{y}\bar{z}$.

Inertial Reference Coordinates

The International Astronomical Union (IAU) standard Earth Mean Equator and Equinox of Besselian 1950.0 inertial reference system (referred to as B1950) is used to define the inertial orientation of $\bar{x}\bar{y}\bar{z}$ as a function of time.[12] The relationship between the body-fixed coordinates and the inertial coordinates is defined by the transformation T^I_{BF} from B1950 ($\bar{X}\bar{Y}\bar{Z}$) to $\bar{x}\bar{y}\bar{z}$ as a function of three rotation angles representing the right ascension α and declination δ of the spin axis of Phobos, and also the hour angle W of the prime meridian. The transformation T^I_{BF} from B1950 ($\bar{X}\bar{Y}\bar{Z}$) to $\bar{x}\bar{y}\bar{z}$ is given by[12]

$$T^I_{BF} = [W]_3[90-\delta]_1[\alpha+90]_3 \tag{19}$$

where T^I_{BF} is a 3×3 orthogonal rotation matrix and the form $[\theta]_i$ represents a 3×3 rotation matrix of angle θ about ith axis ($i = 1$, 2, or 3) as expressed by

$$[\theta]_1 = \begin{pmatrix} 1 & 0 & 0 \\ 0 & \cos\theta & \sin\theta \\ 0 & -\sin\theta & \cos\theta \end{pmatrix}, \quad [\theta]_2 = \begin{pmatrix} \cos\theta & 0 & -\sin\theta \\ 0 & 1 & 0 \\ \sin\theta & 0 & \cos\theta \end{pmatrix}$$

$$[\theta]_3 = \begin{pmatrix} \cos\theta & \sin\theta & 0 \\ -\sin\theta & \cos\theta & 0 \\ 0 & 0 & 1 \end{pmatrix}$$

TV Camera Coordinates

A camera-fixed xyz coordinate system is defined with x on the face of the vidicon and in the direction of increasing sample number, y on the face of the vidicon and in the direction of increasing line number, and z completing the orthogonal, right-hand system and along the optical axis. The origin of the camera-fixed xyz is on the face of the vidicon and located at the optical principal point.

To define the camera pointing and orientation in B1950, the following transformation T^I_{TV} from B1950 ($\bar{X}\bar{Y}\bar{Z}$) to xyz as a function of three rotation angles representing the right ascension α_c and declination δ_c of the optical axis (camera z axis), and the orientation angle κ of camera axes x-y about z, is given by

$$T^I_{TV} = [\kappa]_3[90-\delta_c]_1[\alpha_c+90]_3 \tag{20}$$

Image (Picture) Coordinates

Each of the Viking Orbiter twin TV cameras had a 1.4×1.7 deg field of view and each camera was scanned using 1056 lines with 1204 pixels per line. Given a vector d, where

$$d = (d_x\, d_y\, d_z)^T \tag{21}$$

in TV xyz coordinates, the vidicon (x,y) coordinates associated with d, assuming no optical distortions, are defined by[9]

$$\begin{pmatrix} x \\ y \end{pmatrix} = \frac{f}{d_z} \begin{pmatrix} d_x \\ d_y \end{pmatrix} \tag{22}$$

The sample and line coordinates (s,l) associated with the vidicon (x,y) coordinates, computed for an object viewed through the optics or for a reseau whose vidicon coordinates have been measured, are given by

$$\begin{pmatrix} s \\ l \end{pmatrix} = K(x,y) + \begin{pmatrix} s_0 \\ l_0 \end{pmatrix} \tag{23}$$

where s_0 and l_0 are the image coordinates of the central reseau, which is assumed to be the optical principal point, and $K(x,y)$ is the transformation from vidicon coordinates to sample and line coordinates.[13]

Transforming Points on Reference Surface to Images in the Picture

From Eq. (19), transforming a vector $\bar{b}$ in B1950 to $\bar{u}$ in $\bar{x}\bar{y}\bar{z}$ is accomplished by

$$\bar{u} = T^I_{BF}\bar{b} = T^I_{BF} \begin{pmatrix} b_{\bar{X}} \\ b_{\bar{Y}} \\ b_{\bar{Z}} \end{pmatrix} \tag{24}$$

Therefore, transforming $\bar{u}$ to $\bar{b}$ is

$$\bar{b} = T^{BF}_I \bar{u} \tag{25}$$

where T^{BF}_I, also a 3×3 orthogonal rotation matrix, is the transpose (inverse) of T^I_{BF}. Note that $\bar{b}$ is defined as a surface feature position vector with respect to the center of Phobos in the B1950 system as follows:

$$\bar{b} = \bar{a} - \bar{t} \tag{26}$$

Here, $\bar{t}$ can be derived from the spacecraft and Phobos ephemerides as follows:

$$\bar{t} = \bar{s} - \bar{x} \tag{27}$$

From Eqs. (20) and (26), transforming the surface feature position vector (with respect to spacecraft in B1950) $\bar{a}$ to d in TV xyz coordinates is given by

$$d = T^I_{TV}(\bar{b} + \bar{s} - \bar{x}) \tag{28}$$

From Eqs. (25) and (28), transforming $\bar{u}$ in Phobos body-fixed $\bar{x}\bar{y}\bar{z}$ coordinates to d in TV xyz coordinates is given by

$$d = T^I_{TV} T^{BF}_I \bar{u} + T^I_{TV}(\bar{s} - \bar{x}) \tag{29}$$

Note that d can be transformed from the vidicon (x,y) coordinates in the millimeter space to the image (s,l) coordinates in the sample and line space as shown in Eqs. (22) and (23). Therefore, from Eqs. (21-23) and (29), a vector $\bar{u}$ in Phobos body-fixed $\bar{x}\bar{y}\bar{z}$ coordinates can be transformed to a point (s,l) in the image plane. This is the foundation for processing the surface features using the control network.

Parameter Estimation

The Phobos control network was used to establish the cartographic coordinates of surface features on Phobos.[10] The picture coordinates of the control point images were measured

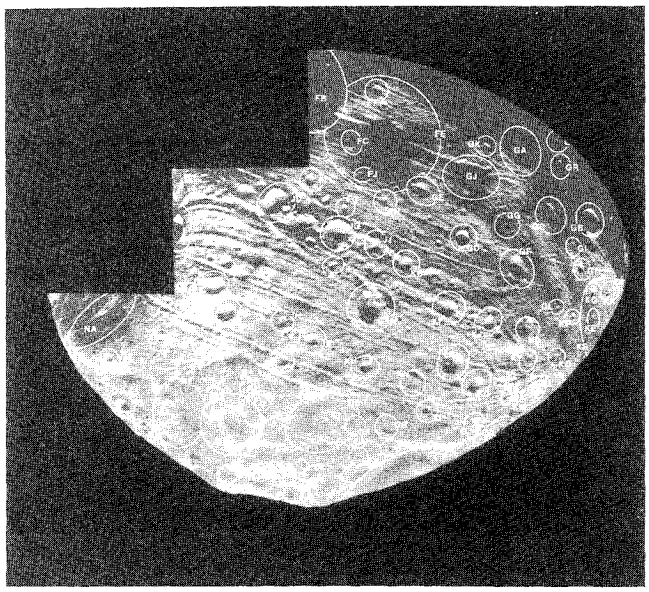

Fig. 2 Identification of Phobos control points in Viking Orbiter images.

interactively using a display of the digital data on a frame buffer.[10] Over 100 Phobos pictures with a total of 542 control points were measured. Each control point was observed at least twice, from different directions. An example of identifying Phobos control points on Viking Orbiter images is given in Fig. 2.

In this example, it is assumed that there is no ephemeris error and that the spacecraft orbit, Phobos orbit, and Mars gravity field were not estimated in the orbit determination process. Instead, the parameters to be estimated were the cartographic coordinates ϕ, λ, u for each control point, the camera pointing and orientation angles α_c, δ_c, κ for each picture, and modeled corrections to the pole and prime meridian angles α, δ, W. An ephemeris of Phobos was determined using data from over 100 years of Earth-based observations, as well as Mariner 9 and Viking imaging data.[10] This process also included corrections to the spacecraft positions as well.

The initial values of ϕ, λ, and u were taken as the average values of the control point latitude, longitude, and radius from the image location measurement process. (All of the data sets used in this example were defined relative to the B1950 system. A future application of this concept should use the data sets that are defined in the new IAU standard Earth Mean Equator and Equinox of J2000 inertial reference system.) The initial values of α, δ, and W were taken from Ref. 10.

A priori camera pointing angles for each picture were obtained from the tracking data and also from star images when available. All camera parameters were determined using hundreds of star images prior to the image location measurement process.

Using the a priori values just mentioned, the predicted image locations of each control point were computed in order to generate residuals and linear partial derivatives for the parameter estimation process. The total number of parameters to be estimated was about 2000. However, because of the stochastic nature of camera pointing angles, the backward smoothing algorithm was used to reduce the problem to about 1650 parameters. This feature will be important in future missions where thousands of pictures will have to be processed. Therefore, the coordinates of surface features (control points) were the largest set of parameters to be estimated.

This problem had n (<1650) unknowns with m ($>4n$) data equations (observables) and was solved using a combination of a square-root information filter (SRIF) and a backward smoothing algorithm. (The conjugate gradient iterative method has also been used by other researchers[14-16] to solve large control network problems. In general, the control network was divided into several overlapping blocks. The normal equations in each block were solved to adjust points in the overlapping regions. The block adjustment processes were performed iteratively until all of the control point coordinates in the overlapping regions converged.[14,15]) SRIF was used to form the upper triangular square-root information matrix from the normal equations for minimizing the computer memory space and also to obtain the solutions for numerical precision and stability.[6-8] With the use of backward smoothing algorithm and the SRIF solutions, more than 300 additional camera pointing angles were obtained.

A batch-sequential data processing algorithm was used for parameter estimation. The control points identified in each picture were grouped as a data batch. Because the camera pointing angles were assumed to be random from picture to picture, the information related to camera pointing angles in the data equations was saved at the end of each batch for later use in the backward smoothing process. The series of steps performed in the parameter estimation process is summarized as follows:

1) The initial values and the appropriate level of uncertainties are selected for the estimated parameters. These uncertainties are used to initialize the SRIF array.

2) For each batch (one batch = one picture), the following steps are performed to accumulate data into the SRIF array.

Predicted image locations of each control point are computed as follows: Compute the body-fixed position vector $\bar{u}$ using Eq. (18). Transform $\bar{u}$ to $\bar{b}$ in the B1950 system using Eq. (25). Input the spacecraft and Phobos positions with respect to Mars in B1950. Transform $(\bar{b}+\bar{s}-\bar{x})$ to $\boldsymbol{d}$ in TV camera coordinates using Eq. (28). Compute image locations (s,l) using Eqs. (22) and (23).

Linear partial derivatives of sample and line image coordinates with respect to the estimated parameters are computed as follows: Compute camera pointing partials by

$$\frac{\partial(s,l)}{\partial(\alpha_c,\delta_c,\kappa)} = \frac{\partial(s,l)}{\partial(x,y)} \frac{\partial(x,y)}{\partial(d_x,d_y,d_z)} \frac{\partial(d_x,d_y,d_z)}{\partial(\alpha_c,\delta_c,\kappa)}$$

Compute pole and prime meridian partials by

$$\frac{\partial(s,l)}{\partial(\alpha,\delta,W)} = \frac{\partial(s,l)}{\partial(x,y)} \frac{\partial(x,y)}{\partial(d_x,d_y,d_z)} \times \frac{\partial(d_x,d_y,d_z)}{\partial(b_{\bar{X}},b_{\bar{Y}},b_{\bar{Z}})} \frac{\partial(b_{\bar{X}},b_{\bar{Y}},b_{\bar{Z}})}{\partial(\alpha,\delta,W)}$$

Compute cartographic coordinates partials by

$$\frac{\partial(s,l)}{\partial(\phi,\lambda,u)} = \frac{\partial(s,l)}{\partial(x,y)} \frac{\partial(x,y)}{\partial(d_x,d_y,d_z)} \frac{\partial(d_x,d_y,d_z)}{\partial(b_{\bar{X}},b_{\bar{Y}},b_{\bar{Z}})} \times \frac{\partial(b_{\bar{X}},b_{\bar{Y}},b_{\bar{Z}})}{\partial(u_{\bar{x}},u_{\bar{y}},u_{\bar{z}})} \frac{\partial(u_{\bar{x}},u_{\bar{y}},u_{\bar{z}})}{\partial(\phi,\lambda,u)}$$

Residuals are computed by differencing the measured and predicted image locations.

The data reduction (or data fitting process) is carried out using a square-root information filter to accumulate the linear partial derivatives and residuals into an upper triangular square-root information matrix.

3) Information that is related to the camera pointing angles for each picture is saved at the end of each batch process using Eq. (10). The data array saved will be used in the backward smoothing process to obtain the corrections to camera pointing angles for each corresponding picture. After saving the camera pointing information, these values are reinitialized to zero except that the diagonal elements are assigned values equal to the reciprocals of the a priori sigmas of camera pointing angles (see Eq. 11). The resulting SRIF array is used to process the next picture.

4) After picture data processing is completed, the corrections to the pole and prime meridian parameters and the cartographic coordinates for all of the control points processed are obtained by inverting the augmented SRIF array. The square-root of the error covariance $\Gamma^{1/2}$ for the estimated parameters is saved for producing the cartographic contour map of Phobos.

5) With the solutions obtained in step 4 and the camera pointing information saved in step 3, the backward smoothing algorithm is applied to obtain the corrections to camera pointing angles for all of the pictures.

6) The resulting solutions for the estimated parameters as shown in steps 4 and 5 may then be used to reinitialize step 1, and the series of subfunctions (steps 1-6) may be carried out iteratively until the solution adjustment converges.

This problem required about 4.0×10^6 double precision words (16 MBytes) of virtual memory on a VAX 11/780 computer and over 24 h of CPU for each of the three iterations performed. It is anticipated that advances in computer technology will enable this same problem to be solved in minutes by the mid-1990s. It is noted that existing supercomputers could do the processing in about 1 h.

Cartographic Accuracy of Phobos

The square-root of the error covariance $\Gamma^{1/2}$ saved for the Phobos control network was used to compute the mapped absolute error covariance for each control point as follows:

$$\Psi_i = \left(\frac{\partial \bar{u}_i}{\partial(\lambda,\phi,u)_i}\right)^T \Lambda_i \frac{\partial \bar{u}_i}{\partial(\lambda,\phi,u)_i}, \qquad i = 1,\ldots,nc \tag{30}$$

where $\partial\bar{u}_i/\partial(\lambda,\phi,u)_i$ is the transformation matrix from cartographic coordinates to body-fixed position vector for the ith control point.

The uncertainty associated with the ith control point σ_i was computed by

$$\sigma_i = \sqrt{\Psi_i^2(1,1)+\Psi_i^2(2,2)+\Psi_i^2(3,3)} \tag{31}$$

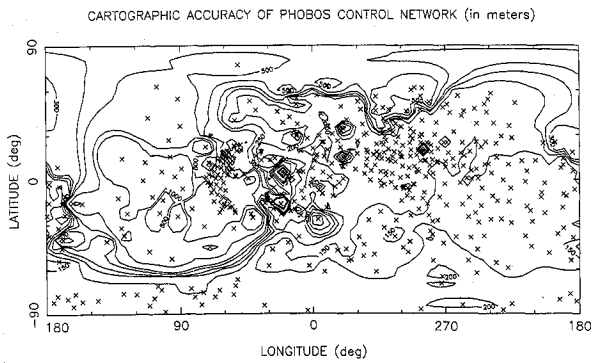

Fig. 3 Cartographic accuracy (in meters) of Phobos in a Mercator projection.

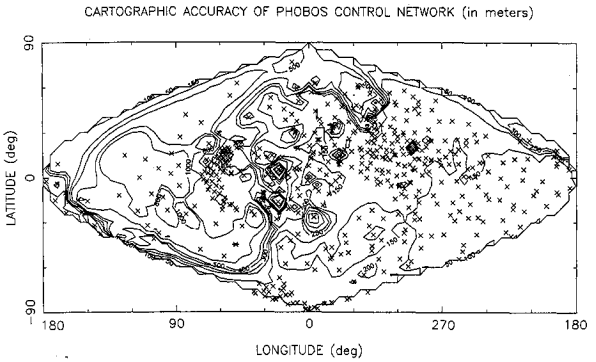

Fig. 4 Cartographic accuracy (in meters) of Phobos in a sinusoidal projection.

These uncertainties along with cartographic coordinates of each control point were used to generate a contour map of the entire Phobos surface. Note that the control points are not evenly distributed. In order to produce a contour map of the entire surface, a set of evenly spaced grid points on latitude and longitude coordinates had to be generated for our contour plotters. It is assumed that the contribution of the control point uncertainties to the uncertainty of a given grid point is inversely proportional to the fourth power of the angular separation between the grid point and each control point. The grid point uncertainty was computed by interpolating each control point uncertainty as follows:

$$\sigma_k = \frac{\sum_{i=1}^{nc} \sigma_i/\vartheta_{ik}^4}{\sum_{i=1}^{nc} 1/\vartheta_{ik}^4} \qquad k = 1,\ldots,ng \tag{32}$$

where σ_i is the level of uncertainty for the ith control point as defined in Eq. (31), and ϑ_{ik} the angle between the control point unit position vector $\hat{u}_i$ and the grid point unit position vector $\hat{u}_k$ and is computed by

$$\vartheta_{ik} = \cos^{-1}(\hat{u}_i \cdot \hat{u}_k) \tag{33}$$

Figure 3 shows the surface features (534 control points) selected in the Phobos control network and the accuracy of the resultant processing displayed on a contour map. The x marks shown in Fig. 3 are the locations of the Phobos control points. Using a sinusoidal map projection,[17,18] the results shown in the contour map of Fig. 3 are displayed in Fig. 4. These maps are needed to determine the level of cartographic accuracy for selecting landing sites.

In addition to these maps, topographic maps of Phobos can also be generated using spherical harmonic expansion[11,19] of the radius to the Phobos surface in terms of cartographic coordinates. A digital terrain model[17] (DTM), which is a computer file of radius or measurement uncertainty data at the discrete latitude and longitude grid points, was used to generate cartographic and topographic maps of Phobos. The DTM maps of Phobos in a sinusoidal projection are given in Fig. 5. The DTM topographic map on the top as shown in Fig. 5 was generated using a topographic model for the surface of Phobos, which includes an eighth degree and order harmonic expansion model and Stickney and crater models.[19] The Stickney and crater models are used to better fit Stickney and other large craters. The results of using Stickney and crater models at the control points are shown in the middle of Fig. 5. The corresponding DTM cartographic accuracy is shown in the

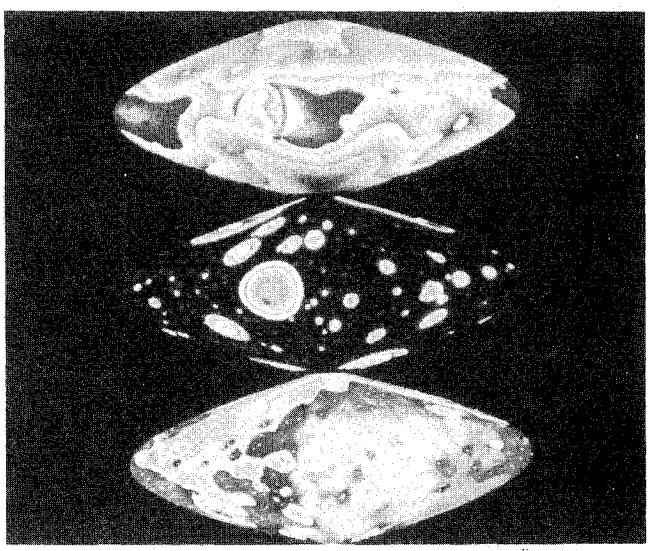

Fig. 5 Maps of Phobos using a digital terrain model.

bottom of Fig. 5. Using the combination of topographic maps and cartographic accuracy maps, a favorable landing site can be selected for targeting landers and penetrators.

Conclusions

Onboard orbital optical navigation data can be used to generate topographic maps for selecting a landing site. The accuracy for these maps depends on the success of a near-real time orbit determination process that solves for a large set of parameters including cartographic coordinates of surface features and camera pointing and orientation angles of each picture. This new approach for targeting landers, rovers, and penetrators using orbital optical navigation in a near-real time operation deserves further study. Future work should include studies using supercomputers to solve large orbit determination problems in near-real time operational environments.

The schemes presented are expected to yield mapping accuracies at the meter level. If the mapping accuracies are relaxed from the meter level, the measurement accuracies of the control points can also be relaxed proportionately. This can be achieved by either reducing the spatial resolution of the imaging cameras or by using simpler image measurement schemes.

Since the relative topographic information is more important than absolute information for selecting a landing site, future work should also include generating maps of the relative cartographic accuracy in the areas where the potential landing sites are to be selected.

Acknowledgments

This work was carried out at the Jet Propulsion Laboratory, California Institute of Technology, Pasadena, California, under contract to NASA. The authors would like to thank Chuck Acton, Manager of the JPL Navigation Ancillary Information Facility (NAIF) for providing the NAIF Toolkit, SPICELIB. The data and image analysis was performed at NAIF. The authors would also like to thank Peter Breckheimer, Eric Cannell, and Ian Underwood of JPL for reviewing this paper and for valuable discussions.

References

[1]Draper, R. F., "The Mariner Mars II Program," AIAA Paper 88-0067, Jan. 1988.

[2]Bourke, R. D., Kwok, J. H., and Friedlander, A., "Mars Rover Sample Return Mission" AIAA Paper 89-0417, Jan. 1989.

[3]Carter, P. H., and Smith, R. S., "Mars Rover Sample Return Lander Performance," AIAA Paper 89-0633, Jan. 1989.

[4]Pivirotto, D. S., Penn, T. J., and Dias, W. C., "Mars Rover 1988 Concepts," AIAA Paper 89-0419, Jan. 1989.

[5]Miller, J. K., Weeks, C. J., and Wood, L. J., "Orbit Determination of the Comet Rendezvous/Asteroid Flyby Mission: Post-Rendezvous," AIAA Paper 89-0348, Jan. 1989.

[6]Wang, T. C., Collier, J. B., Ekelund, J. E., and Breckheimer, P. J., "Applications of Square-Root Information Filtering and Smoothing in Spacecraft Orbit Determination," *Proceedings of the 27th IEEE Conference on Decision and Control,* Vol. 1, IEEE Control Systems Society, 1988, pp. 825–830.

[7]Bierman, G. J., *Factorization Methods for Discrete Sequential Estimation,* Academic, New York, 1977.

[8]Bierman, G. J., and Bierman, K. H., "Estimation Subroutine Library User's Guide (Preliminary)," Factorized Estimation Applications, Inc., Studio City, CA, Rept. 81584, Aug. 1984.

[9]Synnoft, S. P., Donegan, A. J., Riedel, J. E., and Stuve, J. A., "Interplanetary Optical Navigation: Voyager Uranus Encounter," AIAA Paper 86-2113-CP, Aug. 1986.

[10]Duxbury, T. C., and Callahan, J. D., "Phobos and Deimos Control Networks," *Icarus,* Vol. 77, No. 2, 1989, pp. 275–268.

[11]Duxbury, T. C., "The Figure of Phobos," *Icarus,* Vol. 78, No. 1, 1989, pp. 169–180.

[12]Davies, M. E., et al., "Report of the IAU/IAG/COSPAR Working Group on Cartographic Coordinates and Rotational Elements of Planets and Satellites: 1985," *Celestial Mechanics,* Vol. 39, No. 1, 1986, pp. 103–113.

[13]Gaskell, R. W., "Digital Identification of Cartographic Control Points," *Photogrammetric Engineering and Remote Sensing,* Vol. 56, No. 6, 1988, pp. 723–727.

[14]Davies, M. E., and Arthur, D. W. G., "Martian Surface Coordinates," *Journal of Geophysical Research,* Vol. 78, No. 20, 1973, pp. 4355–4394.

[15]Davies, M. E., Hauge, T. A., Katayama, F. Y., and Roth, J. A., "Control Networks for the Galilean Satellites: November 1979," The RAND Corporation, Santa Monica, CA, R-2532-JPL/NASA, Nov. 1979.

[16]Davies, M. E., Colvin, T. R., Katayama, F. Y., and Thomas, P. C., "The Control Networks of the Satellites of Uranus," *Icarus,* Vol. 71, No. 1, 1987, pp. 137–147.

[17]Batson, R. M., "Digital Cartography of the Planets: New Methods, Its Status and Its Future," *Photogrammetric Engineering and Remote Sensing,* Vol. 53, No. 9, 1987, pp. 1211–1218.

[18]Edwards, K., "Geometric Processing of Digital Images of the Planets," *Photogrammetric Engineering and Remote Sensing,* Vol. 53, No. 9, 1987, pp. 1219–1222.

[19]Duxbury, T. C., "An Analytic Model for the Phobos Surface," *Journal of Planetary and Space Sciences,* Vol. 39, No. 1/2, Jan./Feb. 1991, pp. 355–376.